JOURNAL OF SOLID STATE CHEMISTRY **130,** 290–301 (1997)
ARTICLE NO. SC977340

High-Resolution Electron Microscopy Investigations on the Real Structure of $In_5Mo_{18}O_{28}$

R. Ramlau

Max-Planck-Institut für Festkörperforschung, Heisenbergstraße 1, 70569 Stuttgart, Germany

Received October 1, 1996; in revised form January 31, 1997; accepted February 6, 1997

$In_5Mo_{18}O_{28}$, a reduced ternary molybdenum oxide in the series $M_{n\pm\delta}Mo_{4n+2}O_{6n+4}$ with $n = 4$, is a cluster compound containing $Mo_{4n+2}O_{8n+10}$ clusters with $n = 4$ *trans* edge-sharing molybdenum octahedra. A crystal of the compound was investigated by high-resolution electron microscopy (HREM) and related methods, and a comprehensive description of real-structure phenomena is given. These phenomena include: (i) the existence of two ordered polytypes (modifications), 1*M* and 2*O*, which may intergrow with each other, (ii) stacking disorder, and (iii) polysynthetic twinning of the 1*M* polytype. In both ordered polytypes, ordered and disordered chemical intergrowth of $Mo_{4n+2}O_{8n+10}$-cluster layers with $n = 3$, 5, and 6 is observed. Structure models were generated for both modifications in order to have available sets of input data for the simulation of HREM images and electron diffraction intensities. Discrepancies between the results obtained by electron microscopy and by recent single-crystal x-ray structure analysis are discussed. © 1997 Academic Press

INTRODUCTION

The recently synthesized compound $In_5Mo_{18}O_{28}$ (1) is a representative of the reduced ternary and quaternary molybdenum oxides in which condensed clusters built from molybdenum octahedra are arranged in layers of composition $M_{n\pm\delta}Mo_{4n+2}O_{6n+4}$, where n denotes the number of fused, *trans* edge-sharing molybdenum octahedra in the "oligomeric" cluster. Known representatives of this class include $BaMo_6O_{10}$ (2) with $n = 1$, $La_2Mo_{10}O_{16}$ (3) with $n = 2$, $Tl_{1.6}Sn_{1.2}Mo_{14}O_{22}$ (4) with $n = 3$, $Ba_3Mo_{18}O_{28}$ (5) with $n = 4$, and $In_6Mo_{22}O_{34}$ (6) with $n = 5$. An up-to-date formulation and discussion of the general concept of cluster condensation is given elsewhere (7).

The indium oxomolybdates represent a special subset of the reduced ternary oxomolybdates with the formula mentioned above for the layer composition modified to $In_{n+1}Mo_{4n+2}O_{6n+4}$. They constitute a homologous series with known representatives for $n = 4$ (1) and $n = 5$ (6). The series comprises the interesting compound $In_{11}Mo_{40}O_{62}$ (8), which can be rewritten as $In_5Mo_{18}O_{28} \cdot In_6Mo_{22}O_{34}$ indicating that it is composed of alternating cluster layers with $n = 4$ and $n = 5$, respectively.

It is noticed that all the compounds under consideration crystallize in only two space groups, either $P2_1/a$ or *Pnam*, with $In_{11}Mo_{40}O_{62}$, which crystallizes in space group $P2_1am$, being an exception. An overview of literature data is given in Table 1. Two examples taken from this table, one with $n = 3$ and space group $P2_1/a$, the other with $n = 5$ and space group *Pnam*, are displayed in Fig. 1 in selected crystal projections—with the oxygen atoms being omitted for the sake of clarity. An individual $Mo_{4n+2}O_{8n+10}$ cluster and the interconnection of cluster ends via Mo–O–Mo bridges is shown in Fig. 2. This interconnection can vary such that the position of adjacent top and bottom layers is either *trans*, as in Fig. 1a, or *cis*, as in Fig. 1b.

$In_{11}Mo_{40}O_{62}$ was the subject of an early study (14) by high-resolution electron microscopy (HREM) which revealed chemical intergrowth of layers consisting of differently sized clusters. According to the structure principles sketched above, $In_5Mo_{18}O_{28}$ should have a layered structure, with the layers consisting of 4-membered oligomeric clusters. Since the layer composition is hardly differing when n is varied around 4, intergrowth layers of longer or shorter clusters are expected to occur. HREM is an excellent means to investigate such intergrowth structures as well as other structural defects which cannot be recognized with x-ray methods but may influence the results of structure refinements with x-ray data. In the present paper we report the first comprehensive microstructural characterization by HREM devoted to a representative of the ternary or quaternary reduced oxomolybdates. Moreover, our results obtained for $In_5Mo_{18}O_{28}$ will give many indications on the real structure which must be encountered when studying related compounds.

EXPERIMENTAL

Crystals of $In_5Mo_{18}O_{28}$ were prepared via solid state reaction (1). Preliminary characterization on a Buerger-Precession camera revealed that a well-shaped crystal

0022-4596/97 $25.00

TABLE 1
Reduced Molybdenum Oxides in the Series $M_{n\pm\delta}Mo_{4n+2}O_{6n+4}$

Compound	n	Space group	Lattice parameters	Reference
$BaMo_6O_{10}$	1	*Pnam*	$a = 1.0154$ nm, $b = 0.9184$ nm, $c = 0.8641$ nm	(2)
$La_2Mo_{10}O_{16}$	2	$P2_1/a$	$a = 0.9912$ nm, $b = 0.9093$ nm, $c = 0.7575$ nm, $\beta = 109.05°$	(3)
$Sn_2Mo_{10}O_{16}$	2	$P2_1/a$	$a = 0.9970$ nm, $b = 0.9268$ nm, $c = 0.7533$ nm, $\beta = 109.73°$	(9)
$Gd_2Mo_{10}O_{16}$	2	$P2_1/a$	$a = 0.9923$ nm, $b = 0.8993$ nm, $c = 0.7559$ nm, $\beta = 109.81°$	(10)
$Pb_2Mo_{10}O_{16}$	2	$P2_1/a$	$a = 0.9993$ nm, $b = 0.9247$ nm, $c = 0.7536$ nm, $\beta = 109.39°$	(11)
$Tl_{1.6}Sn_{1.2}Mo_{14}O_{22}$	3	$P2_1/a$	$a = 0.9972$ nm, $b = 0.9362$ nm, $c = 1.0362$ nm, $\beta = 104.14°$	(4)
$K_3Mo_{14}O_{22}$	3	$P2_1/a$	$a = 0.9916$ nm, $b = 0.9325$ nm, $c = 1.0439$ nm, $\beta = 103.96°$	(12)
$K_{1.66}Pb_{1.34}Mo_{14}O_{22}$	3	$P2_1/a$	$a = 0.9917$ nm, $b = 0.9276$ nm, $c = 1.0356$ nm, $\beta = 103.83°$	(12)
$K_{1.29}Sn_{1.71}Mo_{14}O_{22}$	3	$P2_1/a$	$a = 0.9929$ nm, $b = 0.9294$ nm, $c = 1.0338$ nm, $\beta = 104.13°$	(12)
$Ba_3Mo_{18}O_{28}$	4	$P2_1/a$	$a = 0.9939$ nm, $b = 0.9377$ nm, $c = 1.3057$ nm, $\beta = 100.92°$	(5)
$In_{11}Mo_{40}O_{62}$	4, 5	$P2_1am$	$a = 0.9883$ nm, $b = 0.9513$ nm, $c = 2.8878$ nm	(8)
$In_6Mo_{22}O_{34}$	5	*Pnam*	$a = 0.9880$ nm, $b = 0.9512$ nm, $c = 3.1767$ nm	(6)
$K_{0.19}Ba_{3.81}Mo_{22}O_{34}$	5	$P2_1/a$	$a = 0.9908$ nm, $b = 0.9353$ nm, $c = 1.5951$ nm, $\beta = 98.78°$	(13)

selected for electron microscopy investigations was not a single crystal (15). It could not be classified in one of the space groups. Fine fragments of the selected crystal were produced by crushing in an agate mortar, then suspended in *n*-butanol and fixed on a holey carbon film. HREM and selected-area electron diffraction (SAD) investigations were performed with a Philips CM30/SuperTWIN electron microscope equipped with a LaB_6 cathode. At 300 kV the point resolution was 0.19 nm. Using the 2.3-mm grids and the respective specimen holder a maximum tilt of $\pm 25°$ was possible in two directions. SAD patterns were taken using a selected area diaphragm which made the diffraction

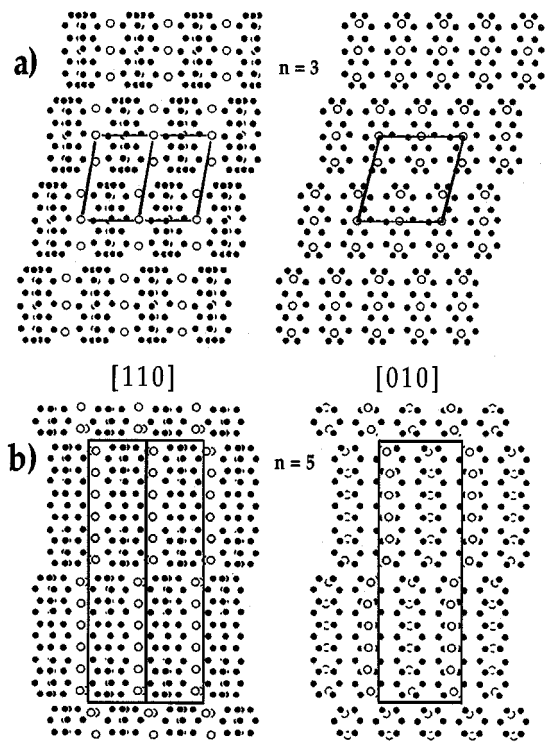

FIG. 1. The structures of (a) the monoclinic $K_3Mo_{14}O_{22}$ (12) with $n = 3$ and (b) the orthorhombic $In_6Mo_{22}O_{34}$ (6) with $n = 5$ projected along the [1 1 0] (left) and the [0 1 0] (right) orientation. Unit cells are indicated. Solid circles denote Mo, open circles K or In, respectively; O is neglected.

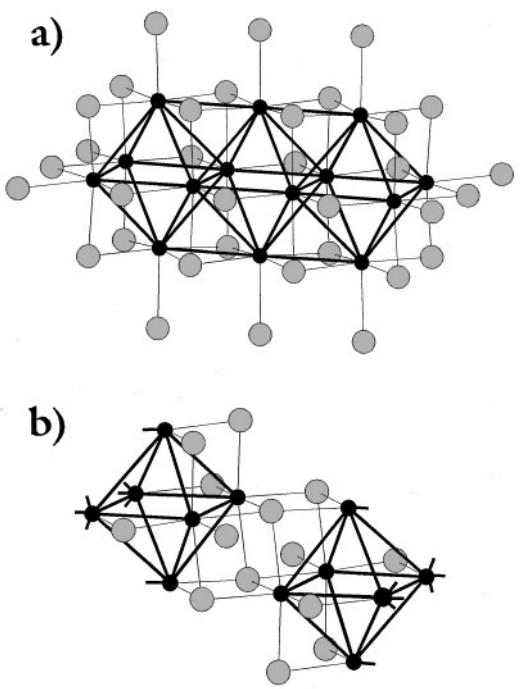

FIG. 2. (a) Structural representation of an individual $Mo_{4n+2}O_{8n+10}$ cluster, here with $n = 3$ for example. Due to interconnection the oxygen content changes to $Mo_{4n+2}O_{6n+4}$ in the respective compounds. Part of this interconnection, the connection of cluster ends, is depicted in (b). Solid circles denote Mo, shaded circles O.

information originate from a specimen region 250 nm in diameter. Series of images at different defocus values ("defocus series"), regarded as absolutely necessary for the correct interpretation of experimental HREM results, were registered whenever the positional stability of the specimen allowed it. Complementary electron probe microanalysis (EPMA) by energy dispersive x-ray spectroscopy (EDXS) was carried out using a Noran HP-Ge detector with ultra-thin window and a Voyager-I system.

Kinematical electron diffraction (ED) patterns were simulated with a program based on the source PATTERN (16), whereas the EMS program package (17) was used for both the simulation of HREM images and the calculation of dynamical ED intensities—with exit-wave functions calculated according to the multislice formalism. The spherical aberration constant C_S amounted to 1.15 mm, the defocus spread parameter was $\Delta = 7$ nm, and the illumination semiangle was determined to be $\alpha = 1.2$ mrad. The latter value may appear a little too high compared with values commonly given for the microscope used. However, under the conditions chosen (cathode heating, spot size, condenser-2 diaphragm) any further lowering of α by defocussing the condenser system led to an inacceptable increase of the exposure time.

The existence of amorphous surface layers on the crystal fragments and the appearance of a beam-induced structure transformation were two factors which complicated HREM. In order to reduce the influence of amorphous surface layers, all of the HREM images reproduced in this paper were Fourier filtered applying the GATAN Digital-Micrograph software. The beam-induced transformation is—at least in the thinner regions of the specimen—obviously associated with the migration of the In atoms out of the crystal and their deposition on the specimen surface. Under the illumination conditions generally applied for our HREM imaging (current density $j \approx 30\ \mathrm{A\,cm^{-2}}$) the very thin regions at the edges of crystal fragments are completely transformed within minutes. It should be emphasized that this process does not, in any way, affect the cluster length n and the stacking of cluster layers. A similar phase transformation occurred when studying compounds in the $Sn_xMo_{10}O_{16}$–$Sn_yMo_{14}O_{22}$ system by HREM (18).

RESULTS

At appropriate orientations of the crystal fragments, HREM images reveal the existence of two kinds of domains. They differ primarily in the stacking sequences of their cluster layers; that is, either *ABCDA* or *ABABA*. Of course, these sequences differ from the stacking of close-packed layers of spheres, where only 3 layer positions are possible, but relate to layer stacking in general polytypic structures. The stacking sequence *ABCDA* is characteristic of the reduced oxomolybdates crystallizing in space group $P2_1/a$, whereas the sequence *ABABA* is characteristic of those crystallizing in space groups *Pnam* and $P2_1am$ (cf. Table 1). Since there were no other stacking sequences observed, we denote them as monoclinic and orthorhombic stacking.

It should be mentioned at the very beginning that, in the case of the monoclinic stacking, the *ABCDA* notation is not completely adequate. For all the monoclinic members listed in Table 1 including the monoclinic domains of $In_5Mo_{18}O_{28}$, every cluster layer is shifted by nearly exactly $\boldsymbol{a}/4$ with respect to its preceding layer. The error $(4 \cdot c \cdot \cos(180^\circ - \beta) - a)/a$, with a, c, and β being monoclinic lattice parameters, is always in the range between -2% and $+2\%$. Hence, every fifth layer projects—in a rather good approximation—onto the first, when viewing along the cluster axes, which are almost parallel to [1 0 4].

Both monoclinic and orthorhombic domains can be more or less extended (Figs. 3–5). They vary from a few cluster layers to sizes covering an entire crystal fragment (some 100 nanometers). Within the frame of experimental error, EPMA of sufficiently large domains of both types did not

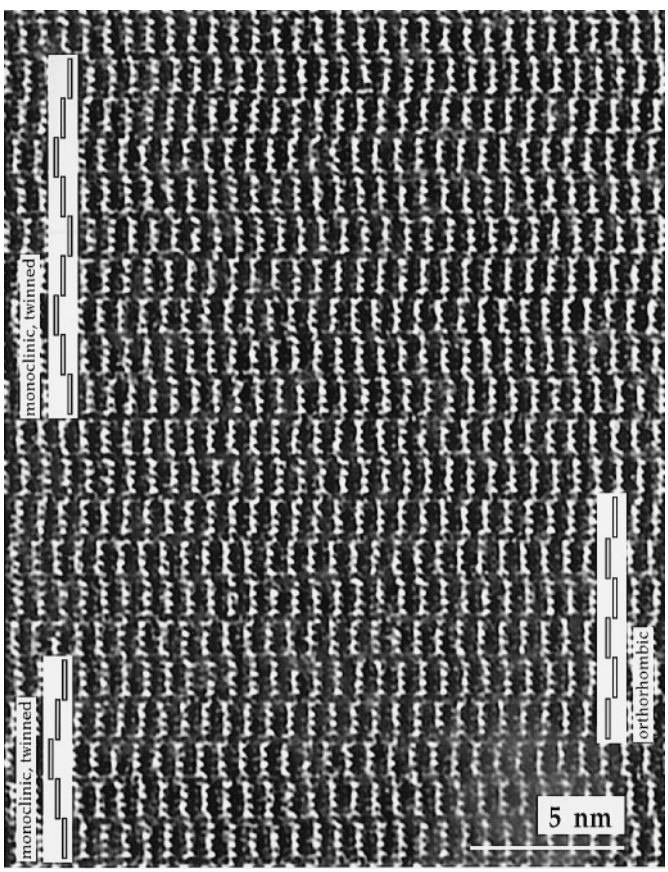

FIG. 3. HREM image of $In_5Mo_{18}O_{28}$ in the [1 1 0] orientation showing stacking disorder. Domains with monoclinic stacking—polysynthetically twinned on a submicroscopic scale—and a domain with orthorhombic stacking are marked on the left and right, respectively.

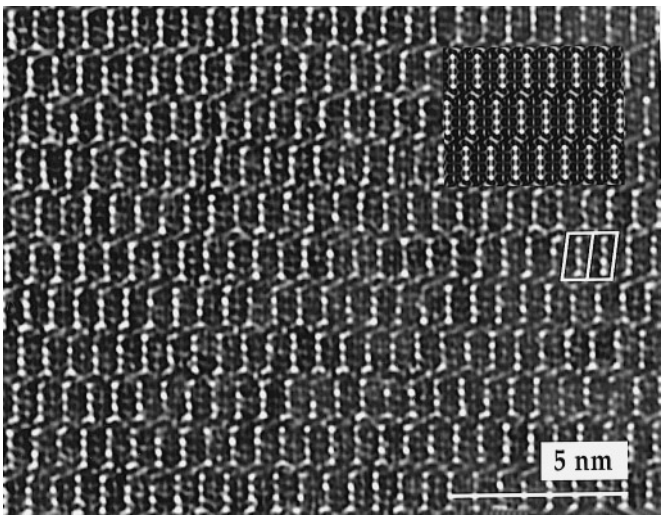

FIG. 4. HREM image of $In_5Mo_{18}O_{28}$ in the [1 1 0] orientation. The extended monoclinic domain displays the stacking sequence *ABCDA* (unit cell indicated). A computer simulated image ($t = 10$ nm, $\Delta f = -100$ nm) is shown as an inset upper right.

reveal any difference in their In/Mo ratio. Their oxygen content could not be determined reliably. Figure 3 shows that the monoclinic domains, which constitute about 70% of the investigated crystal, show a strong tendency for polysynthetic twinning through the (0 0 1) plane. Sometimes, as in Fig. 3, the twin lamellae are only three layers thick, and the full monoclinic stacking sequence *ABCDA* cannot be realized. Although macroscopic twinning may also occur, it is barely observable by HREM of crystal fragments.

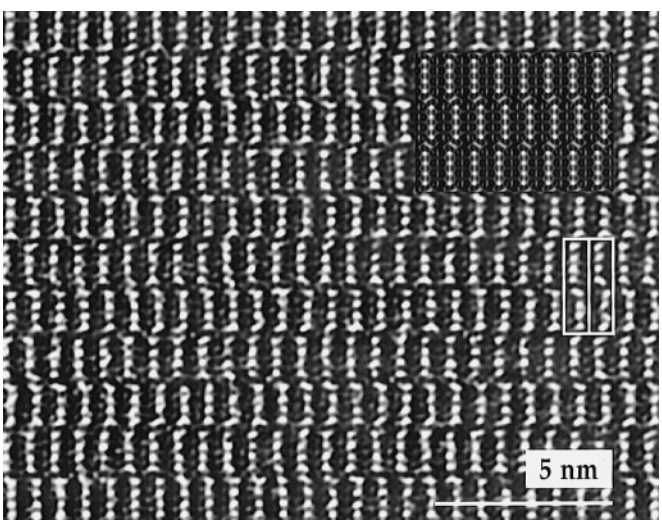

FIG. 5. HREM image of $In_5Mo_{18}O_{28}$ in the [1 1 0] orientation. The extended orthorhombic domain displays the stacking sequence *ABABA* (unit cell indicated). A computer simulated image ($t = 10$ nm, $\Delta f = -100$ nm) is shown as an inset upper right.

Figures 4 and 5 display HREM images of larger domains with monoclinic *ABCDA* and orthorhombic *ABABA* stacking, respectively, in [1 1 0] orientation; the corresponding SAD patterns are shown in Figs. 7b and 8b. Since both types of domains can obviously be relatively large, it has been concluded rather early (19) that $In_5Mo_{18}O_{28}$ occurs in two ordered polytypes, i.e., two polytypic modifications, of which the monoclinic one (Ramsdell symbol: 1*M*) crystallizes in space group $P2_1/a$ and the orthorhombic one (Ramsdell symbol: 2*O*) in *Pnam*. The respective space groups have been postulated by analogy to the related structures that are summarized in Table 1. By the way, it should be mentioned that using these nonstandard settings, most of the prominent zone axes have equivalent indices for both polytypic modifications.

To get data for the computer simulation of HREM images, the "structure principle" of the compounds given in Table 1 was carefully examined and idealized lattice parameters were derived (1*M*: $a = 1.0000$ nm, $b = 0.9500$ nm, $c = 1.3120$ nm, $\beta = 100.89°$; 2*O*: $a = 1.0000$ nm, $b = 0.9500$ nm, $c = 2.5767$ nm). For both modifications of $In_5Mo_{18}O_{28}$, sets of atomic positions—given in Tables 2 and 3—were generated under the assumption that the oligomeric clusters are built from ideal, rigid Mo octahedra, that the In polycations are linearly arranged with constant In–In distances, and that the oxygen atoms can be completely neglected. Figure 6 illustrates the parallel projections of the two polytypic structures in [1 1 0], [0 1 0], and [1 0 0] directions.

Simulations of HREM images carried out on the basis of our crude structure models reflect the overall features of experimental HREM images rather well, although they do not agree exactly in all details. The same holds for the simulated kinematical ED patterns. Simulated HREM images are presented as insets to the experimental HREM images, e.g., in Figs. 4 and 5. For both the 1*M* and the 2*O* polytypes, experimental ED patterns (b) taken from

TABLE 2
Idealized Atomic Coordinates for $In_5Mo_{18}O_{28}$-1*M*

Atom	Wyckoff position	*X*	*Y*	*Z*
Mo(1)	4*e*	0.9735	0.1231	0.0558
Mo(2)	4*e*	0.7531	0.1231	0.1669
Mo(3)	4*e*	0.0286	0.1231	0.2780
Mo(4)	4*e*	0.8082	0.1231	0.3891
Mo(5)	4*e*	0.0837	0.1231	0.5000
Mo(6)	4*e*	0.8633	0.1231	0.6113
Mo(7)	4*e*	0.1388	0.1231	0.7224
Mo(8)	4*e*	0.9184	0.1231	0.8335
Mo(9)	4*e*	0.1939	0.1231	0.9446
In(1)	4*e*	0.3909	0.0000	0.0558
In(2)	4*e*	0.4460	0.0000	0.2780
In(3)	2*c*	0.5000	0.0000	0.5000

TABLE 3
Idealized Atomic Coordinates for $In_5Mo_{18}O_{28}$-2*O*

Atom	Wyckoff position	*X*	*Y*	*Z*
Mo(1)	8*d*	0.0403	0.1231	0.0834
Mo(2)	8*d*	0.0403	0.1231	0.1945
Mo(3)	8*d*	0.4576	0.6230	0.0279
Mo(4)	8*d*	0.2924	0.3769	0.0279
Mo(5)	8*d*	0.2097	0.6230	0.0834
Mo(6)	8*d*	0.4576	0.6230	0.1390
Mo(7)	8*d*	0.2924	0.3769	0.1390
Mo(8)	8*d*	0.2097	0.6230	0.1945
Mo(9)	4*c*	0.4576	0.6230	0.2500
Mo(10)	4*c*	0.2924	0.3769	0.2500
In(1)	8*d*	0.3750	0.0000	0.0279
In(2)	8*d*	0.3750	0.0000	0.1390
In(3)	4*c*	0.3750	0.0000	0.2500

sufficiently extended ordered domains as well as simulated kinematical ED patterns (a) are given in Figs. 7 and 8.

Stimulated by our HREM results, it was possible to identify $In_5Mo_{18}O_{28}$ single crystals of both the monoclinic and orthorhombic polytypic modifications, and full structure analyses have been carried out using x-ray methods (1). The structures were refined in the postulated space groups; lattice parameters are given in Table 4. Unfortunately, the x-ray structure data (1) do not fit the experimental ED patterns, examples of which are displayed in Figs. 7 and 8. The discrepancies between the experimental (b) and the simulated (c) patterns become most obvious when comparing the intensities of a particular pair of reflections, namely (0 0 4) and (0 0 5) in the 1*M* polytype as well as (0 0 8) and (0 0 10) in the 2*O* polytype. Considering the obvious discrepancy between the experimental ED patterns and those simulated on the basis of x-ray data (1), it will not be a surprise to learn that the corresponding HREM images cannot be simulated on the basis of these data, either. Possible reasons for this lack of agreement are discussed in a later paragraph.

The HREM micrographs of Figs. 3–5 were taken in [1 1 0] orientation, which is most suitable to image the stacking of cluster layers directly (cf. also Fig. 6a). It is, however, often difficult to identify the oligomeric clusters as 4-membered—except via metrics or by comparison with computer-simulated images. (For all [1 1 0] images reproduced in this paper, particular defocus values were chosen to provide the impression of *n*-membered units.) On the other hand, the oligomeric clusters themselves can be imaged most instructively in [0 1 0] orientation, but then information on the stacking sequence is essentially lost. In Fig. 6b, which refers to the generated, idealized structure data, one could not at all differentiate between the two projected structures and would get the impression of an orthorhombic (or pseudo-orthorhombic) structure in both cases, if the projection of the unit cells had not been drawn. In experimental [0 1 0] images like those in Fig. 9, the monoclinic or orthorhombic features become discernible only by precise measurement of angles and careful inspection of image details. As the projected structure in Fig. 6c indicates, HREM imaging in [1 0 0] orientation is less instructive. Neither can the stacking sequences be visualized, nor can the cluster length *n* be made out easily. That is why [1 0 0] images are not reproduced in this paper.

Figures 9a–c show some HREM micrographs which are all taken in [0 1 0] orientation from a monoclinic domain,

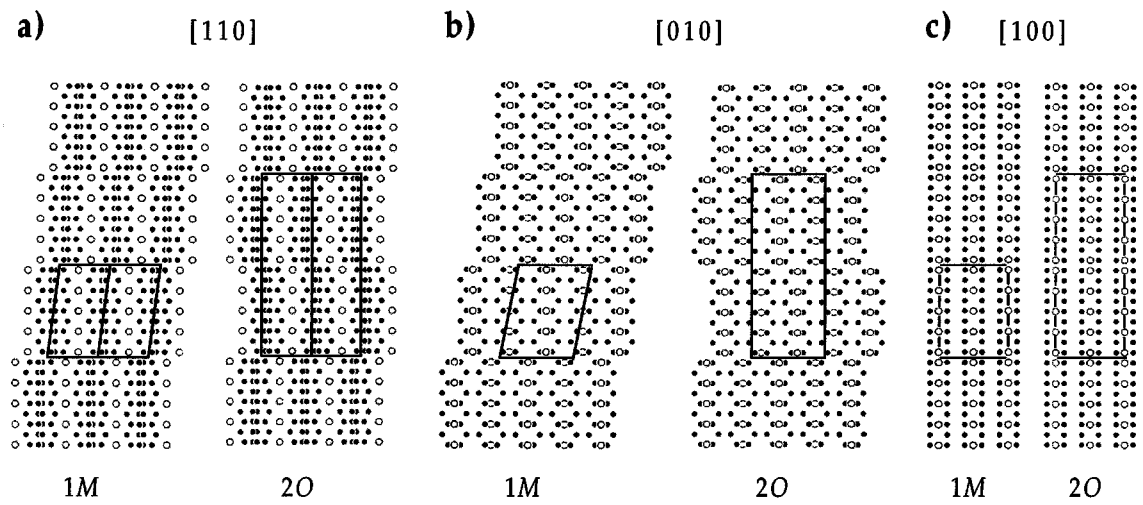

FIG. 6. Projections of the idealized structures (see the text) of $In_5Mo_{18}O_{28}$-1*M* and $In_5Mo_{18}O_{28}$-2*O* along (a) the [1 1 0], (b) the [0 1 0], and (c) the [1 0 0] orientation. Unit cells are indicated. Solid circles denote Mo, open circles In; O is neglected.

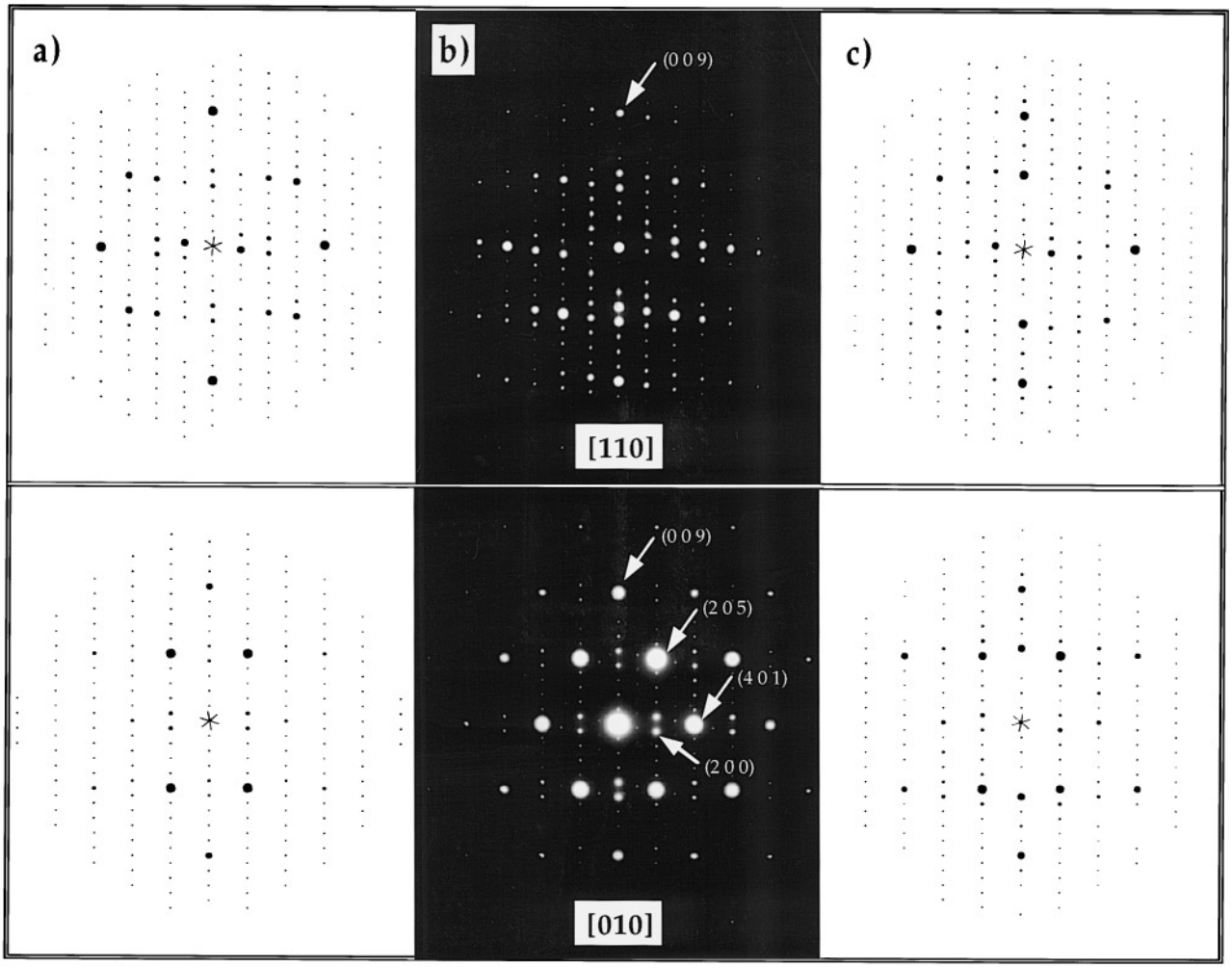

FIG. 7. (b) SAD patterns of large monoclinic domains in $In_5Mo_{18}O_{28}$ for the [1 1 0] and the [0 1 0] orientation, together with kinematical ED patterns simulated on the basis of (a) the idealized structure model (see the text and Table 2) and (c) x-ray data (1).

but with different values of specimen thickness t and defocus Δf. Images, which are computer simulated on the basis of our 1*M* structure model, are inserted for comparison. Figure 9a refers to a rather thin specimen region, and it was taken at *Scherzer* defocus. Under these conditions, heavier atoms or clusters thereof are imaged in black, whereas the spaces between the heavier atoms as well as the spaces between the clusters are imaged in white. The micrograph can be likened to elongated honeycombs consisting of four black hexagons corresponding to four projected Mo octahedra. The less bright spots in the center of each black hexagon represent a view through the Mo octahedra (cf., the projected structures in Fig. 6b). The brighter spots surrounding each honeycomb represent spaces between Mo clusters which are filled with oxygen atoms. Under image conditions (i.e., [0 1 0] orientation, thin specimen, *Scherzer* defocus) applied for the micrograph in Fig. 9a, a microscope with point resolution 0.14 nm would be necessary to resolve the single Mo atoms of the octahedra. In a HREM micrograph such as that given in Fig. 9c, we meet a completely different situation. The centers of the Mo octahedra are now represented by very bright spots, which makes it very easy to determine the cluster length n by counting the number of spots. Computer simulated and experimental images are in good agreement, thus indicating once more the relatively high reliability of our crude structure models.

The occurrence of two ordered polytypes, 1*M* and 2*O*, which are existing in more or less extended domains intergrown with each other, as well as the polysynthetic twinning of the 1*M* domains can be interpreted as phenomena of stacking disorder—at least, when the domains of ordered stacking or the twin domains are very small. In addition to

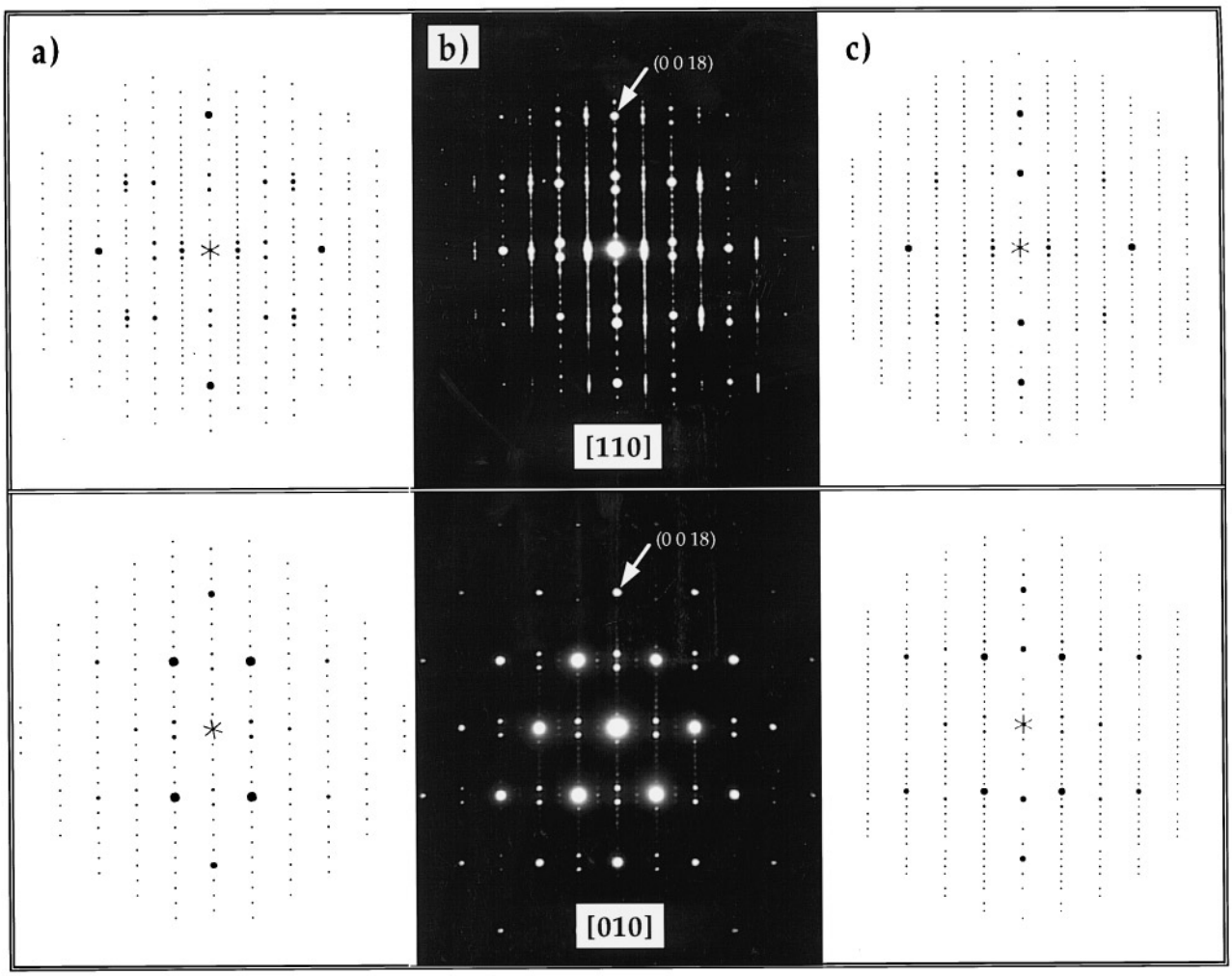

FIG. 8. (b) SAD patterns of large orthorhombic domains in $In_5Mo_{18}O_{28}$ (nominal composition) for the [1 1 0] and the [0 1 0] orientation, together with kinematical ED patterns simulated on the basis of (a) the idealized structure model (see the text and Table 3) and (c) x-ray data (1). The experimental SAD patterns display streaks along (0 0 1) since intergrowth layers consisting of 5-membered oligomeric clusters occur very frequently in orthorhombic domains.

this stacking disorder, HREM revealed chemical intergrowth as an important feature of the investigated crystal. In both the monoclinic (1*M*) and orthorhombic (2*O*) domains, monolayers and multilayers of differently sized clusters have been found. Since these intergrowth structures can themselves exhibit subdomains showing different stacking sequences, a large variety of structural features arises. Only a few examples can be treated here. Figure 10 shows a double layer and two monolayers of 5-membered clusters randomly intergrown into a monoclinic domain of 4-membered clusters. According to the nature of [0 1 0] projections, the stacking sequence can hardly be derived exactly,

TABLE 4
The Two Modifications of $In_5Mo_{18}O_{28}$

Modification	Space group	Lattice parameters	Reference
1*M*	$P2_1/a$	$a = 0.9895$ nm, $b = 0.9519$ nm, $c = 1.3231$ nm, $\beta = 100.98°$	(1)
2*O*	*Pnam*	$a = 0.9896$ nm, $b = 0.9520$ nm, $c = 2.597$ nm	(1)

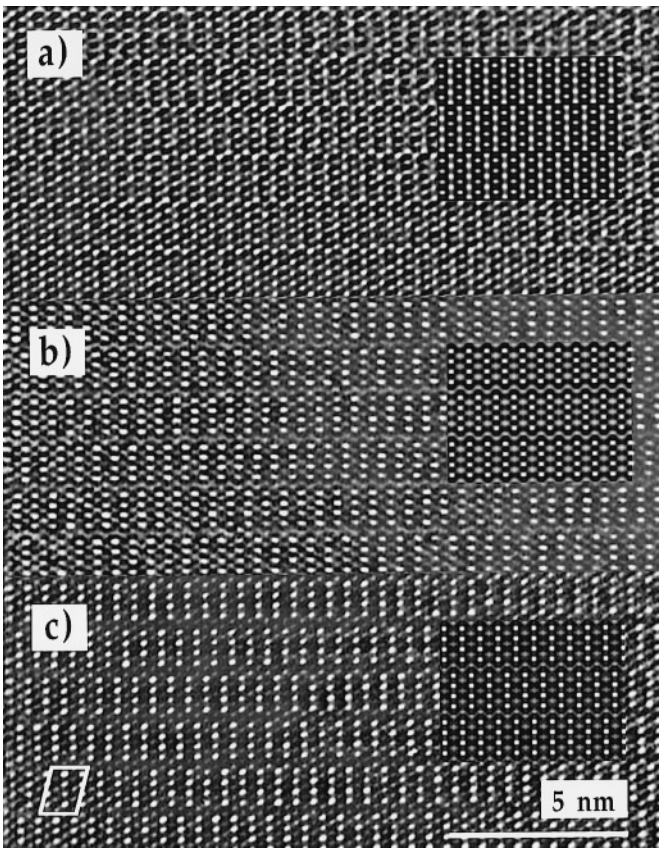

FIG. 9. Monoclinic domain of $In_5Mo_{18}O_{28}$ in the [0 1 0] orientation (unit cell indicated), imaged at different specimen thicknesses and with different defocus values. Computer simulated images are shown as insets: (a) $t = 5$ nm, $\Delta f = -60$ nm, (b) $t = 5$ nm, $\Delta f = -110$ nm, and (c) $t = 10$ nm, $\Delta f = -110$ nm.

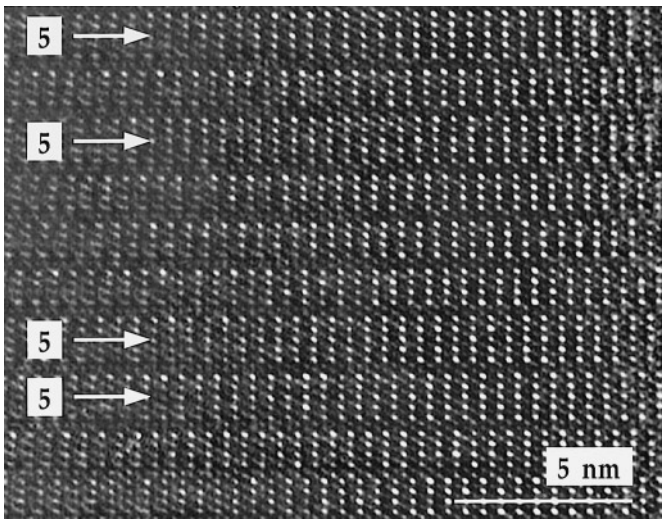

FIG. 10. Monoclinic domain of $In_5Mo_{18}O_{28}$ (nominal composition) in the [0 1 0] orientation with randomly intergrown layers consisting of 5-membered clusters (marked by arrows).

but the corresponding SAD pattern (see Fig. 7b) indicates the monoclinic stacking sequence *ABCDA*.

In general, intergrowth of layers consisting of longer clusters ($n = 5, 6$) is more often observed in domains with orthorhombic than in those with monoclinic stacking sequence. Figure 11 displays an example of ordered chemical intergrowth. Obeying the stacking sequence *ABABA*, every other layer consists of 5-membered clusters. Thus a subdomain of $In_{11}Mo_{40}O_{62} = In_5Mo_{18}O_{28} \cdot In_6Mo_{22}O_{34}$ (cf. Table 1) is formed. Another example of ordered chemical intergrowth obeying the *ABABA* sequence is given in Fig. 12. Layers of 5-membered clusters are dominating and only every fourth layer consists of 4–membered clusters. Consequently, the chemical composition of the considered subdomain is $In_{23}Mo_{84}O_{130} = In_5Mo_{18}O_{28} \cdot 3(In_6Mo_{22}O_{34})$. A SAD pattern taken from a rather extended subdomain of orthorhombic $In_6Mo_{22}O_{34}$, together with an ED pattern simulated on the basis of literature data (6), is displayed in Figs. 13b and 13c. Figure 13a shows part of this subdomain with an intergrown monolayer of 6-membered clusters; this is a little difficult to realize, because the imaged crystallite is rather thick. The intergrowth layer is about 1.9 nm wide, which is about the estimated value of 1.87 nm ($c/2 = 1.59$ nm for $In_6Mo_{22}O_{34}$ plus 0.28 nm as the length of one Mo_6 octahedron). Since monolayers consisting of 6-membered clusters occur only in those subdomains with 5-membered clusters dominating, this is more a phenomenon of chemical intergrowth in $In_6Mo_{22}O_{34}$ than in $In_5Mo_{18}O_{28}$.

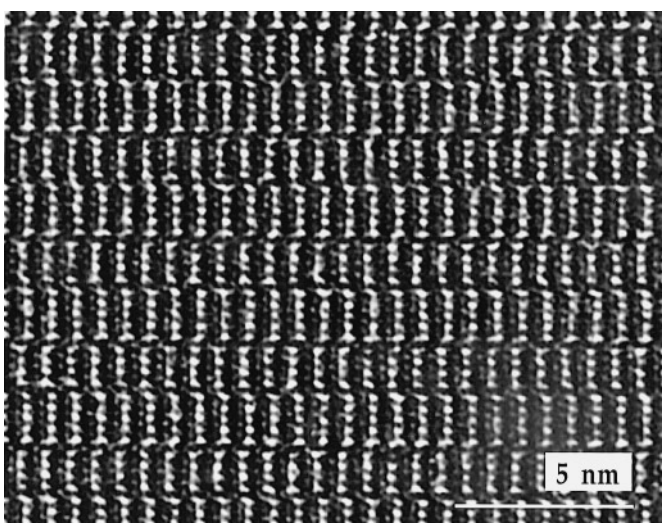

FIG. 11. Orthorhombic domain in the [1 1 0] orientation with layers consisting alternatingly of 4-membered and 5-membered clusters. The ordered intergrowth structure corresponds to the already known compound $In_{11}Mo_{40}O_{62}$ (8).

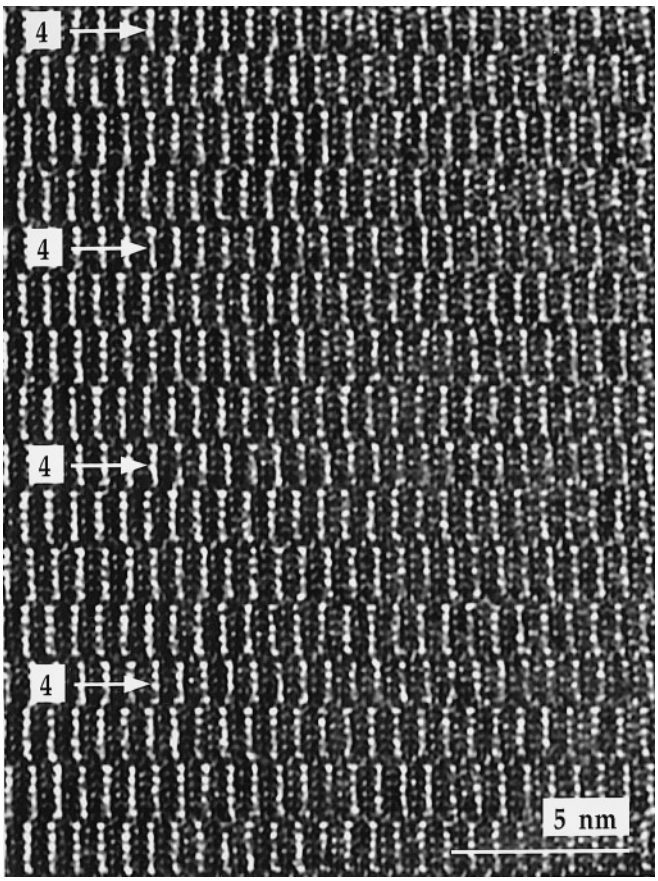

FIG. 12. Orthorhombic domain in the [1 1 0] orientation, in which layers consisting of 5-membered clusters are dominating. Only every fourth layer consists still of 4-membered clusters (marked by arrows). The ordered intergrowth structure has the composition $In_{23}Mo_{84}O_{130}$.

Chemical intergrowth of oligomeric clusters of different lengths within a monoclinic domain is illustrated by Figs. 14 and 15. Figure 14 shows a monolayer consisting of 3-membered clusters intergrown within a matrix with the stacking sequence *ABCDA*. Such intergrown layers of 3-membered oligomeric clusters were scarcely found, and in fact the reduced indium oxomolybdate with $n = 3$, i.e., $In_4Mo_{14}O_{22}$, has not been prepared as a single phase yet. The HREM micrograph of Fig. 15 shows intergrown monolayers of 5-membered oligomeric clusters, likewise following the monoclinic stacking sequence *ABCDA*. Sometimes we observed rather extended subdomains—up to 10 layers—which are formed only of 5-membered clusters stacked with the monoclinic sequence. Therefore, we suggest that the compound with $n = 5$, $In_6Mo_{22}O_{34}$, must not only exist in its 2*O* modification described by Dronskowski *et al.* (6), but also in a 1*M* modification. (A triple-layer of monoclinically stacked 5-membered clusters can be seen in the upper part of Fig. 16.)

The combination of stacking disorder and disordered chemical intergrowth is finally illustrated by Fig. 16. The stacking changes from orthorhombic *ABABA* in the lower part to monoclinic *ABCDA* in the upper part of the micrograph. In both domains monolayers or multilayers consisting of 5-membered clusters are randomly introduced.

DISCUSSION

In the present paper the term "polytypic" is interpreted following the definition given by Guinier *et al.* (20). "An element or compound is *polytypic* if it occurs in several different structural modifications, each of which may be regarded as built up by stacking layers of (nearly) identical structure and composition, and if the modifications differ only in their stacking sequence." To the best of our knowledge the composition of the layers building up the 1*M* and 2*O* polytypes is exactly the same, namely $In_5Mo_{18}O_{28}$.

On the other hand, the layers are not isomorphic in a strict crystallographic sense. As can be learned from the structure data reported by Fais *et al.* (1) as well as from the structures of the other reduced oxomolybdates listed in Table 1, deviations relate mainly to the positions of the cations at the ends of the In_{n+1} chains belonging to each cluster layer and to the positions of those oxygen atoms which make the *inter*cluster coupling. There may be other minor deviations from the strict isomorphism of stacking layers, too. From bonding arguments, it was concluded (1) that four modes of *inter*cluster coupling should be possible, whereas only two are realized in the 1*M* and 2*O* modifications. With four possible modes of *inter*cluster coupling, of course, more than two ordered polytypes would be expected to exists for $In_5Mo_{18}O_{28}$. By our HREM investigations, however, no evidence for more than two modes of *inter*cluster coupling was observed. The additional two, hypothetical modes of *inter*cluster coupling would be, by necessity, connected with adjacent cluster layers being shifted against one another by vectors orthogonal (or nearly orthogonal) to the common shift vectors $\pm \mathbf{a}/4$, but of the same absolute value. Such shifts, if ever existent, could be easily observed in HREM images taken in [0 1 0] or [1 0 0] orientations (indices referring to the 1*M* and 2*O* modifications).

It has already been mentioned in the previous paragraph that experimental SAD patterns and, consequently, experimental HREM images cannot be simulated on the basis of the x-ray data published (1). The discrepancies between experimental and simulated ED patterns are not due to dynamical diffraction effects: First, to realize kinematical diffraction conditions as closely as possible, experimental diffraction patterns have been taken from the thinnest parts of the investigated crystals. Second, using the data of Fais *et al.* (1) dynamical diffraction intensities $I_{(hkl)}$ have been simulated as a function of the crystal thickness t. It proved to be impossible to model the experimental reality (cf. Fig. 17).

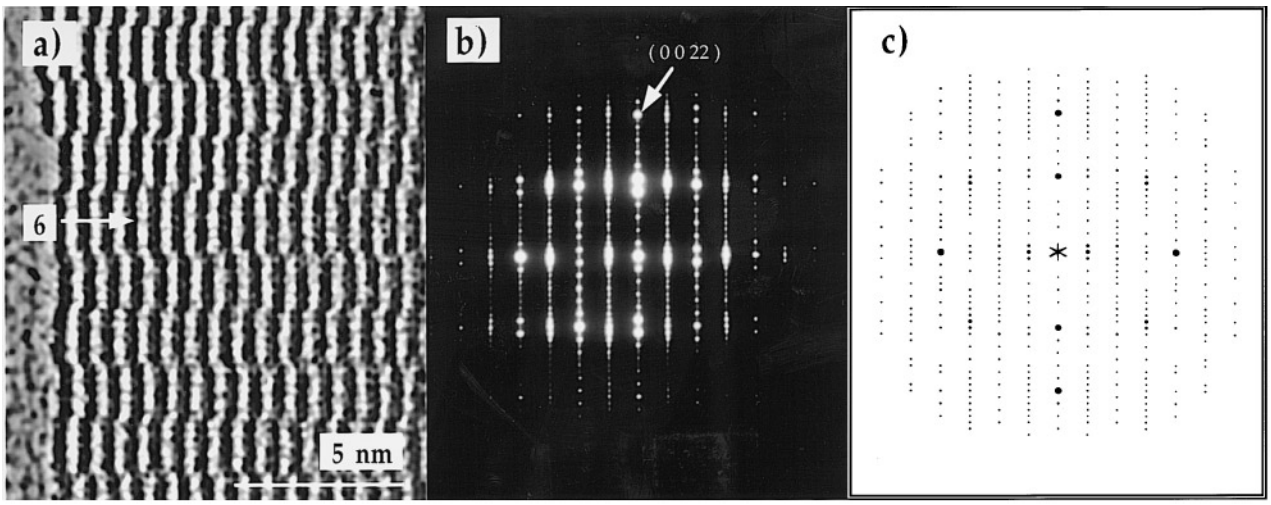

FIG. 13. (a) HREM image of an orthorhombic domain in the [1 1 0] orientation consisting merely of 5-membered clusters with one intergrown monolayer consisting of 6-membered clusters (marked by an arrow); (b) corresponding SAD pattern, and (c) kinematical ED pattern simulated on the basis of x-ray data (6) for the compound $In_6Mo_{22}O_{34}$-2*O*.

A qualitative argumentation should be exemplarily given for the diffraction pattern of the 1*M* polytype in [0 1 0] orientation displayed in Fig. 7b. The primary beam has not been shaded off when recording this pattern. Its rather low intensity, which is comparable to the intensities of the diffracted beams, indicates that the validity range of the kinematical theory of electron diffraction is exceeded and dynamical multibeam excitation must be taken into account. Although the crystallite was not perfectly aligned in the symmetrical Laue orientation, it is evident that

$$I_{(004)} \approx I_{(005)} \approx I_{(200)} \approx I_{(201)} < I_{(009)} \text{ and} \quad [1]$$

$$I_{(401)} \approx I_{(205)} > I_{(009)}. \quad [2]$$

The calculated depth profile of dynamical intensities for some beams of interest is now shown in Figs. 17a and 17b. $I_{(004)} \approx I_{(005)} \approx I_{(200)} \approx I_{(201)}$ seems never to be fulfilled. In any case, $I_{(004)}, I_{(005)}, I_{(200)}, I_{(201)} < I_{(009)}$ holds only

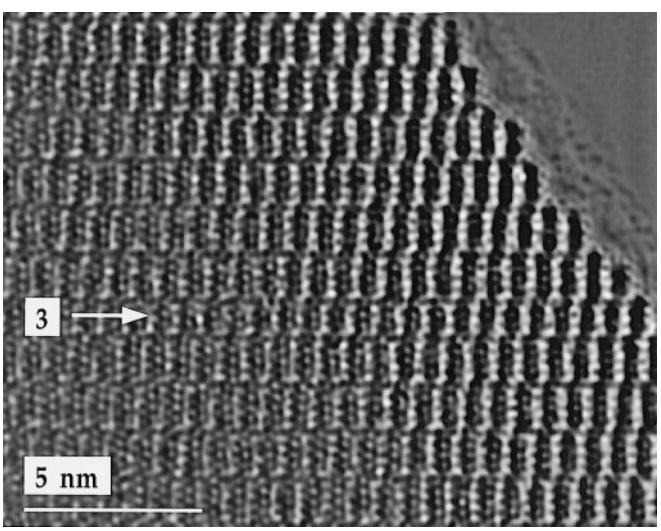

FIG. 14. Monoclinic domain of $In_5Mo_{18}O_{28}$ in the [1 1 0] orientation with an intergrown monolayer (marked by an arrow) consisting of 3-membered clusters.

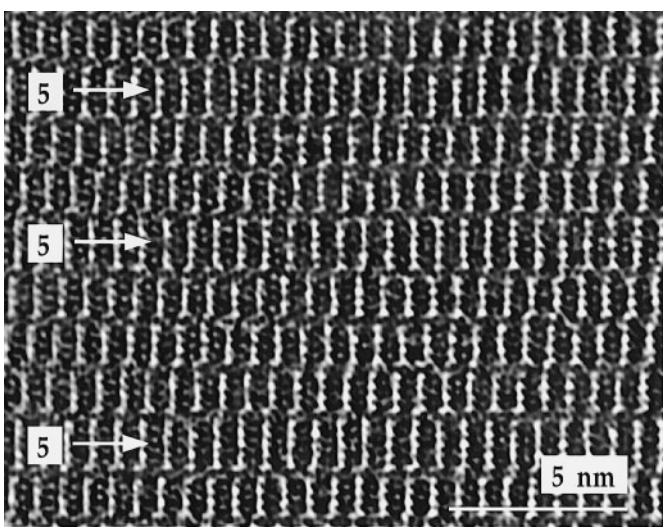

FIG. 15. Monoclinic domain in the [1 1 0] orientation with randomly intergrown monolayers (marked by arrows) consisting of 5-membered clusters.

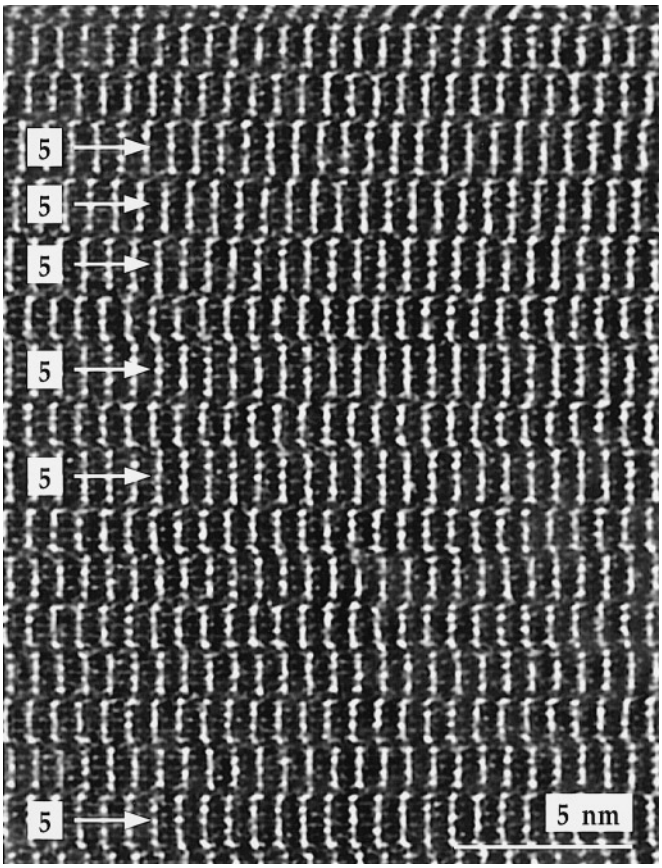

FIG. 16. HREM image in the [1 1 0] orientation showing the combination of stacking disorder and disordered chemical intergrowth. In both the orthorhombic (lower part) and the monoclinic (upper part) domains, layers consisting of 5-membered clusters (marked by arrows) are randomly intergrown.

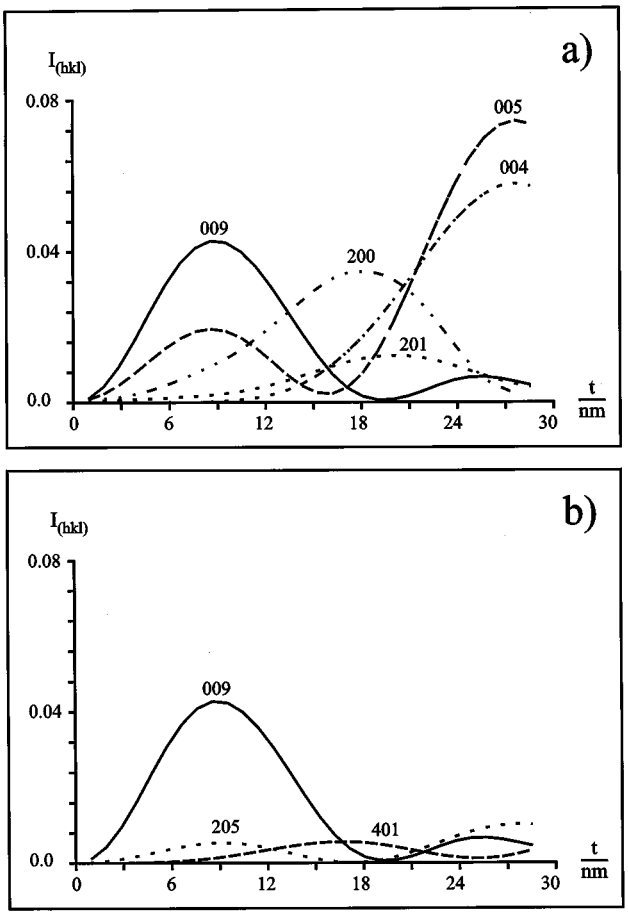

FIG. 17. Dynamical multibeam ED intensities $I_{(hkl)}$ as a function of the specimen thickness t for $In_5Mo_{18}O_{28}$-1M in the [0 1 0] orientation, simulated on the basis of x-ray data (1). The intensity of the incident electron beam is taken as unity. For the sake of clarity, some reflections (*hkl*) of particular interest are displayed in two different diagrams. A corresponding SAD pattern is given in Fig. 7b.

for $t < 13.5$ nm. On the other hand, condition [2] is only fulfilled for 19.5 nm $< t <$ 22.0 nm. Consequently conditions [1] and [2] cannot be satisfied for any reasonable crystal thickness.

Another cause for the observed discrepancies may be seen in the beam-induced phase transformation which takes place when the investigated microcrystallites are irradiated in the electron microscope. SAD patterns can, however, be registered without prior irradiating the specimen region of interest. This is realized by tilting the microcrystallite into the desired orientation while it is irradiated in a certain region. When alignment is perfect one switches to an adjacent region—not irradiated before—to take a SAD pattern. The experimental SAD patterns displayed in Figs. 7 and 8 are observed at the very beginning of electron irradiation. A change in the diffraction patterns, which originate from an area 250 nm in diameter, can be noticed after about 5 min of irradiation with a current density of $j \approx 30$ A cm^{-2} (whereas the transformation proceeds much faster in the thin regions at the edges of a specimen, which are suited for taking HREM micrographs). The beam-induced phase transformation, which is also observed when irradiating reduced tin oxomolybdates, will be the subject of a separate publication (21).

Having in mind the abundance of structural features revealed by HREM, which include polytypism, stacking disorder, polysynthetic twinning on a submicroscopic scale, and chemical intergrowth of layers consisting of other oligomeric clusters, it seems most likely that the crystals used for x-ray structure investigations and refinement were subject to such disorder, too.

CONCLUSIONS

By HREM it became evident that $In_5Mo_{18}O_{28}$ occurs in two ordered polytypes, 1M and 2O, which mainly differ in

the stacking sequence of their cluster layers, *ABCDA* and *ABABA*. There is no evidence for the existence of further ordered polytypes. In real crystals more or less extended domains of both ordered polytypes can be intergrown. If the respective domains are very small, disordered polytypes are formed. The 1*M* polytype shows a strong tendency to polysynthetic twinning on a submicroscopic scale through the (0 0 1) plane.

Due to the fact that the compositions of reduced ternary indiumoxomolybdates $In_{n+1}Mo_{4n+2}O_{6n+4}$ with n varying around 4 are rather similar, in both the 1*M* and 2*O* domains, intergrowth layers consisting of shorter ($n = 3$) or longer ($n = 5, 6$) clusters are observed. These intergrowth layers occur as monolayers or multilayers, sometimes randomly and sometimes introduced in an ordered manner. In the case of ordered chemical intergrowth of layers consisting of 5-membered clusters, domains of different phases are formed, e.g., of $In_{11}Mo_{40}O_{62}$ (8). In the case of chemical intergrowth of multilayers consisting of 5-membered clusters, domains of $In_6Mo_{22}O_{34}$ (6) are formed. Since these $In_6Mo_{22}O_{34}$ domains likewise occur with two different stacking sequences, *ABCDA* and *ABABA*, it is suggested that there should exist two polytypic modifications of $In_6Mo_{22}O_{34}$, instead of the one (2*O*) published (6). Moreover, it may be presumed that polytypism is common to all the representatives of the series $M_{n\pm\delta}Mo_{4n+2}O_{6n+4}$ with $n \geq 4$.

The SAD patterns for both 1*M*-$In_5Mo_{18}O_{28}$ and 2*O*-$In_5Mo_{18}O_{28}$ lack agreement with ED patterns simulated on the basis of x-ray structure data (1). The disagreement may be due to imperfect single crystals used for x-ray structure investigations. Since very complex features of real structure, which—on a submicroscopic scale—combine intergrowth of different ordered polytypes, polysynthetic twinning and chemical intergrowth, were observed by HREM, it seems very difficult to grow perfect single crystals of $In_5Mo_{18}O_{28}$. To avoid the experimental restrictions and incertitudes coming up from the electron-beam induced phase transformation of all the reduced indium oxomolybdates, it seemed promising to devote a HREM study to those of the compounds listed in Table 1 with rather immobile counter cations (22).

ACKNOWLEDGMENTS

The author is deeply indebted to Professor Arndt Simon, who spent funds from his Leibniz-Award to procure the electron microscopy equipment, suggested the work reported in the present paper, and was always ready for discussions. Dr. Hansjürgen Mattausch is gratefully acknowledged for initiation in the field of oxomolybdates, Dipl.-Chem. Eva Fais for making available the investigated crystallite, and Miss Viola Duppel for assistance with the photographic work.

REFERENCES

1. E. Fais, H. Borrmann, Hj. Mattausch, and A. Simon, *Z. Anorg. Allg. Chem.* **621,** 1178 (1995).
2. K. H. Lii, C. C. Wang, and S. L. Wang, *J. Solid State Chem.* **77,** 407 (1988).
3. S. J. Hibble, A. K. Cheetham, A. R. L. Bogle, H. R. Wakerley, and D. E. Cox, *J. Am. Chem. Soc.* **110,** 3295 (1988).
4. R. Dronskowski and A. Simon, *Angew. Chem. Int. Ed. Engl.* **28,** 758 (1989).
5. G. L. Schimek, D. E. Nagaki, and R. E. McCarley, *Inorg. Chem.* **33,** 1259 (1994).
6. R. Dronskowski, Hj. Mattausch, and A. Simon, *Z. Anorg. Allg. Chem.* **619,** 1397 (1993).
7. A. Simon, *in* "Clusters and Colloids" (G. Schmid, Ed.), pp. 373–458. Verlag Chemie, Weinheim, 1994.
8. Hj. Mattausch, A. Simon, and E.-M. Peters, *Inorg. Chem.* **25,** 3428 (1986).
9. P. Gougeon, M. Potel, and M. Sergent, *Acta Crystallogr. C* **46,** 1188 (1990).
10. P. Gougeon, P. Gall, and M. Sergent, *Acta Crystallogr. C* **47,** 421 (1991).
11. R. Dronskowski, A. Simon, and W. Mertin, *Z. Anorg. Allg. Chem.* **602,** 49 (1991).
12. G. L. Schimek, S. C. Chen, and R. E. McCarley, *Inorg. Chem.* **34,** 6130 (1995).
13. G. L. Schimek and R. E. McCarley, *J. Solid State Chem.* **113,** 345 (1994).
14. A. Simon, W. Mertin, Hj. Mattausch, and R. Gruehn, *Angew. Chemie. Int. Ed. Engl.* **25,** 845 (1986).
15. E. Fais, Thesis, University of Stuttgart, Stuttgart, 1995.
16. R. A. Ploc and G. H. Keech, *J. Appl. Crystallogr.* **5,** 244 (1972).
17. P. A. Stadelmann, *Ultramicroscopy* **21,** 131 (1987).
18. R. Ramlau, G. Schimek, R. E. McCarley, and A. Simon, *Z. Anorg. Allg. Chem.* **622,** 437 (1996).
19. R. Ramlau, E. Fais, Hj. Mattausch, and A. Simon, *Optik* **94,** Suppl. 5, 70 (1993).
20. A. Guinier *et al.*, *Acta Crystallogr. A* **40,** 399 (1984).
21. R. Ramlau, A. Simon, and R. E. McCarley, in preparation.
22. R. Ramlau, R. E. McCarley, and A. Simon, in preparation.